Research in Astronomy and Astrophysics manuscript no.
(LaTeX: output.tex; printed on April 21, 2022; 17:26)

Candidate eclipsing binary systems with a δ Scuti star in Northern TESS field

F. Kahraman Aliçavuş[1,2], D. Gümüş[3], Ö. Kırmızıtaş[4], Ö. Ekinci[5], S. Çavuş[4], Y. T. Kaya[6] and F. Aliçavuş[1,2]

[1] Çanakkale Onsekiz Mart University, Faculty of Sciences and Arts, Physics Department, 17100, Çanakkale, Turkey; *filizkahraman01@gmail.com*

[2] Çanakkale Onsekiz Mart University, Astrophysics Research Center and Ulupnar Observatory, TR-17100, anakkale, Turkey

[3] Istanbul University, Institute of Graduate Studies in Science, Programme of Astronomy and Space Sciences,34116, Beyazıt,Istanbul, Turkey

[4] Çanakkale Onsekiz Mart University, School of Graduate Studies, Department of Physics, TR-17100, anakkale, Turkey

[5] Çanakkale Onsekiz Mart University, School of Graduate Studies, Department of Space Sciences and Technologies, TR-17100, anakkale, Turkey

[6] Çanakkale Onsekiz Mart University, Faculty of Engineering Computer Engineering, TR-17100, anakkale, Turkey

Received 20xx month day; accepted 20xx month day

Abstract Existence of pulsating stars in eclipsing binaries have been known for decades. These types of objects are extremely valuable systems for astronomical studies as they exhibit both eclipsing and pulsation variations. The eclipsing binaries are the only way to directly measure the mass and radius of stars with a good accuracy ($\leq 1\%$), while the pulsations are a unique way to probe the stellar interior via oscillation frequencies. There are different types of pulsating stars existing in eclipsing binaries. One of them is the δ Scuti variables. Currently, the known number of δ Scuti stars in eclipsing binaries is around 90 according to the latest catalog of these variables. An increasing number of these kinds of variables is important to understand the stellar structure, evolution and the effect of binarity on the pulsations. Therefore, in this study, we focus on discovering new eclipsing binaries with δ Scuti component(s). We searched for the northern TESS field with a visual inspection by following some criteria such as light curve shape, the existence of pulsation like variations in the out-of-eclipse light curve and the $T_{\rm eff}$ values of the targets. As a result of these criteria, we determined some targets. The TESS light curves of the selected targets first were removed from the binarity and frequency analysis was performed on the residuals. The luminosity,

absolute and bolometric magnitudes of the targets were calculated as well. To find how much of these parameters represent the primary binary component (more luminous) we also computed the flux density ratio of the systems by utilizing the area of the eclipses. In addition, the positions of the systems in the H-R diagram was examined considering the flux density ratios. As a consequence of the investigation, we defined 38 candidates δ Scuti and also one Maia variable in eclipsing binary systems.

Key words: techniques: photometric : — stars: variables: binaries : eclipsing — stars: variables: δ Scuti star

1 INTRODUCTION

Space telescopes have created a revolution in astronomical studies. The primary mission of some of these telescopes is mainly discovering new exoplanets, however, in addition to their success in finding new exoplanets, they have provided a huge amount of photometric data of stellar systems. Especially, the *Kepler* (Borucki et al., 2010) and the Transiting Exoplanet Survey Satellite (TESS, Ricker et al. 2014) have a big impact on this. TESS has already finished its two-years of primary mission and is currently continuing its extended mission by observing the almost entire sky. The high-quality photometric data of these space telescopes allow us to deeply investigate some phenomena in stellar systems and understand their structures.

To comprehend the evolution and the structure of stars, the eclipsing binaries and the pulsating stars are substantial systems. The eclipsing binaries are the only way to precisely determine the mass (M) and radius (R) parameters of the binary components with the help of modelling the photometric light curves and radial velocity measurements. The accuracy of the measured M and R values can be lower than 1% (Lacy et al., 2015; Southworth, 2013). On the other hand, pulsating stars are unique systems that allow us to probe the stellar interior via oscillation frequencies (Aerts et al., 2010). Thanks to the analysis of high-quality space-based photometric data of pulsating stars we had information on some important phenomena such as internal rotation, core overshooting and angular momentum (e.g. Lovekin & Guzik, 2017; Saio et al., 2015). Therefore, the eclipsing binaries with a pulsating component(s) are such crucial systems for deeply exploring the stellar evolution and structure.

The presence of pulsating stars in eclipsing binaries has been known for decades (Tempesti, 1971). There are different types of oscillating variables present in eclipsing binaries for instance β Cephei, δ Scuti and γ Doradus stars (Lampens, 2021; Southworth, 2021). Currently, the known number of δ Scuti stars in eclipsing binaries is higher than the other type of pulsating variables because of their relatively shorter pulsation periods (Lampens, 2021; Kahraman Aliçavuş et al., 2017; Liakos & Niarchos, 2017). The δ Scuti stars are early A to F type variable and their luminosity class changes from dwarf to giant (Aerts et al., 2010). These variables have their own instability strip where theoretically δ Scuti -type variations are expected (Dupret et al., 2005). The δ Scuti stars generally exhibit pressure mode oscillation with an oscillation period range of 18-min. to 8h (Aerts et al., 2010). According to the recent catalog of δ Scuti stars in eclipsing binaries (DSEB), there are around 90 DSEB (Kahraman Aliçavuş et al., 2017). Additionally, there are also δ Scuti stars present in other types of binary systems (Liakos & Niarchos, 2017).

The effect of binarity on pulsations has been shown in some studies (Handler et al., 2020; Kahraman Aliçavuş et al., 2017; Soydugan et al., 2006; Mkrtichian et al., 2004). Because of the gravitational effects of the components on each other, it was expected that the pulsations in oscillating components differ from single pulsating stars. The effect of binarity on the pulsating δ Scuti components was shown by a relationship between the pulsation and orbital period (Soydugan et al., 2006). It was obtained that the pulsation period (P_{puls}) decreases when the orbital period (P_{orb}) declines. The smaller P_{orb} means that the binary components are closer to each other, so the semi-major axis (a) is shorter. According to the gravity law, applied gravitational force on the pulsating components is increased by the declined P_{orb}. A comparison of the properties of single and eclipsing binary member δ Scuti stars was given by Kahraman Aliçavuş et al. (2017). They showed that P_{puls} and pulsation amplitude (A_{puls}) of single classical δ Scuti stars are longer and higher, respectively, comparing to eclipsing binary member δ Scuti variables. In this study, it was also presented that single δ Scuti stars have a higher rotation velocity ($v \sin i$) on average compared to DSEB. These are the results of the effects of gravitational forces between the binary components. In the same study, lots of relationships were examined between the pulsation properties (P_{puls}, A_{puls}) and other stellar parameters such as M, R, effective temperature ($T_{\rm eff}$) and surface gravity ($\log g$).

In a recent study, by the help of TESS data, Handler et al. (2020) first time showed that in a close binary system the pulsation axis of the oscillating component can be aligned by tidal forces. There are now a few samples of this kind of objects including an eclipsing binary system and they are called to be "Tidally tilted pulsators" (Kurtz et al., 2020; Fuller et al., 2020; Handler et al., 2020). The high-quality TESS data allowed us to find such variables which have been searched for years and has provided a good opportunity to deeply probe DSEB. A comprehensive research of DSEB is quite important for comprehending stellar structure, evolution and testing evolutionary models. For this reason, an increased number of such systems will offer us more opportunities for understanding stellar objects. Hence, in this study, we focus on DSEB.

In this study, we present our TESS northern field research for discovering new δ Scuti stars in eclipsing binaries. The paper is organised as follows. In Sect. 2, information about the observational data and target selection are introduced. In Sect. 3, the frequency analysis of the selected targets is given. In Sect. 4, calculations of some physical parameters and the position of the systems are presented. In Sect. 5 and Sect. 6, discussion and conclusions are given, respectively.

2 OBSERVATIONAL DATA AND TARGET SELECTION

To discover new DSEB we searched for the northern TESS field. TESS was launched in April 2018 and it is the main goal is detecting exoplanets. TESS has four identical CCD cameras that have $24^o \times 24^o$field of view (FOV) (Ricker et al., 2014). TESS monitors the sky with a wide red-bandpass filter by dividing it into sectors. Each sector has around 27 days of photometric observations. In the first two years of the mission, TESS observed many targets with 2-min short cadence (SC) and 30-min long cadence (LC) and now in its extended mission, LC was reduced to 10-min. According to the position of the target in the sky, some objects were observed by TESS in more than one sector while some have only one sector data. The TESS data are public in the Barbara A. Mikulski Archive for Telescopes (MAST)[1] archive where the data

[1] https://mast.stsci.edu

is present in two kinds of flux; the simple aperture photometry (SAP) and the pre-search data conditioning SAP flux (PDCSAP). The PDCSAP fluxes are the long term trends removed fluxes and mostly the cleaner data.

In the current study, to find new eclipsing binaries with a δ Scuti component, we had a visual inspection for all TESS sectors in the northern hemisphere. Basically, in the first step, we searched for eclipsing binary like variations in the TESS data. In the next step, the out-of-eclipse variations of the determined eclipsing binaries were examined and the systems that exhibit both eclipsing binary variations and oscillation like changes in the out-of-eclipse light curves were chosen as targets. In the final step, the atmospheric parameters ($T_{\rm eff}$, $\log g$) of the targets were checked. As δ Scuti components are searched for, we considered that targets which have $T_{\rm eff}$ and $\log g$ parameters in the range given for δ Scuti stars. According to the study of Rodríguez & Breger (2001), typical $T_{\rm eff}$ and $\log g$ ranges for δ Scuti stars are $6300-8500$ K and $3.2-4.3$, respectively. Therefore, for the final list the targets, which have $T_{\rm eff}$ and $\log g$ in the given ranges within errors, were chosen. The atmospheric parameters of the targets were taken from the TESS input catalog (TIC, Stassun et al., 2019). The final list of the targets is given in Table 1. There is one target (TIC 13037534) which has $T_{\rm eff}$ lower than the given $T_{\rm eff}$ for δ Scuti stars even considering a possible error. However, the target illustrates significant δ Scuti -type variations and its spectral type is given as F1V in the catalog of Avvakumova et al. (2013). Considering a possible error in $T_{\rm eff}$ we included this target in our list as well. As a result, we have 39 candidates of DSEB listed in Table 1.

For the analysis of the candidate DSEB, we preferred to use only SC data because the Nyquist frequency for the SC data reaches $\sim$360 d^{-1}. Taking into account the typical frequency range of δ Scuti variables ($\sim$4$-$80 d^{-1} Aerts et al. 2010), the SC data are the most suitable data for an examination of δ Scuti -type variations. In Table 1, the available TESS sectors for each target is given. In our analysis, we used the PDCSAP fluxes and each flux was converted into magnitude.

3 FREQUENCY ANALYSIS

In the current study, our main goal is revealing δ Scuti -type variations in our candidate systems. Therefore, we carried out a frequency analysis for each system. We used the PERIOD04 program which derives individual frequencies from astronomical data including gaps and also allows us to find the combination and harmonic frequencies (Lenz & Breger, 2005). Our analysis consists of two steps. In the first step, the binary variations were removed from all available data of each target to obtain only the variation of oscillations. The binary variations were removed from the data with a phenomenological fit including the frequency of orbital periods and their harmonics (Kahraman Aliçavuş et al., 2022). Before starting this analysis, the orbital periods of each target were calculated by performing a frequency analysis and these orbital periods were used in the current research. We could not determine the orbital periods for some systems because there is only one primary eclipse in their data. The derived orbital parameters are given in Table 1. In Fig. 1, we show one example of orbital period frequency fits to the TESS data and the residuals. As clearly seen from the figure, the binary variations were extracted and only the light curve of the pulsations was obtained. In the light curves of some systems, there are only one or two eclipses in available data. For these systems,

Table 1: The List of Candidate DSEB and Their Properties. The Atmospheric Parameters Were Taken From the TIC (Stassun et al., 2019) and an Average Error is Given For These Parameters.

TIC Number	RA(J2000)	DEC(J2000)	P_{orb} (day)	V (mag)	$T_{\rm eff}$ (K) $\pm$ 181	$\log g$ $\pm$ 0.09	Sectors
8669966	$16^h\ 33^m\ 29^s.1$	$+30^o\ 29'\ 56".6$	3.400272 (6)	6.89	7651	3.54	25
10057647	$08^h\ 53^m\ 19^s.3$	$+53^o\ 44'\ 08".9$	16.259725 (5)	8.52	7249	4.06	20, 47
13037534[a]	$22^h\ 55^m\ 30^s.2$	$+64^o\ 00'\ 31".0$	30.220888 (9)	11.29	5694	–	17, 18, 24
14948284	$12^h\ 41^m\ 07^s.8$	$+30^o\ 26'\ 13".6$	2.699312 (8)	6.95	7178	3.86	22
48084398	$18^h\ 47^m\ 29^s.6$	$+49^o\ 25'\ 55".3$	4.243430 (7)	7.20	6814	3.29	14, 15, 26, 40
71613490	$13^h\ 29^m\ 56^s.1$	$+34^o\ 31'\ 27".4$	1.313542 (7)	7.69	7737	3.84	23
72839144[b]	$16^h\ 56^m\ 28^s.7$	$+37^o\ 39'\ 18".9$	1.755764 (2)	10.03	7189	3.68	25
75593781[c]	$05^h\ 41^m\ 34^s.9$	$+25^o\ 59'\ 52".9$	1.532149 (6)	11.39	8300	4.33	43, 44, 45
78148497	$05^h\ 54^m\ 24^s.5$	$+26^o\ 18'\ 31".7$	2.708848 (5)	10.96	7287	3.93	43, 45
85600400	$17^h\ 16^m\ 49^s.9$	$+38^o\ 21'\ 58".7$	1.471461 (5)	12.19	7235	3.85	25, 26
116334565	$05^h\ 40^m\ 28^s.4$	$+30^o\ 58'\ 27".3$	3.475191 (7)	11.32	7546	3.60	43, 45
165618747	$17^h\ 20^m\ 07^s.8$	$+13^o\ 39'\ 57".6$	0.648264 (3)	11.67	7603	4.11	25, 26
172431974	$19^h\ 58^m\ 50^s.1$	$+39^o\ 19'\ 52".1$	2.387408 (3)	10.96	7236	3.71	14, 15, 41
193774939[d]	$17^h\ 53^m\ 12^s.7$	$+43^o\ 46'\ 23".2$	1.305766 (7)	10.16	7358	4.05	25, 26
197755658[e]	$22^h\ 28^m\ 01^s.7$	$+53^o\ 41'\ 00".1$	3.158785 (4)	11.46	7645	3.86	16, 17
197757000[f]	$22^h\ 28^m\ 49^s.9$	$+53^o\ 46'\ 15".9$	2.185923 (7)	11.10	6985	3.92	16, 17
240962482	$01^h\ 15^m\ 58^s.9$	$+52^o\ 46'\ 40".0$	4.475000 (1)	10.12	7748	3.81	18
241013310	$01^h\ 20^m\ 12^s.8$	$+48^o\ 36'\ 41".4$	2.144879 (6)	10.11	7093	4.01	17, 18
256640561	$21^h\ 51^m\ 35^s.4$	$+71^o\ 53'\ 08".7$	1.712080 (2)	8.41	7891	3.48	17, 18, 24, 25
272822330	$23^h\ 46^m\ 17^s.9$	$+62^o\ 01'\ 33".4$	4.501230 (4)	10.06	7340	3.56	17, 18, 24
289947843	$06^h\ 40^m\ 16^s.6$	$+79^o\ 35'\ 58".3$	–	6.75	9175	4.12	19, 20, 26, 40, 47
301909087[g]	$02^h\ 41^m\ 16^s.5$	$+48^o\ 56'\ 18".8$	4.448759 (6)	10.81	6847	3.54	18
305633328	$21^h\ 02^m\ 23^s.9$	$+60^o\ 04'\ 41".9$	2.506158 (3)	11.76	6899	–	16, 17
322428763	$18^h\ 35^m\ 03^s.3$	$+28^o\ 49'\ 40".1$	6.714251 (8)	11.18	6151	3.27	40
327121759[h]	$00^h\ 13^m\ 30^s.1$	$+58^o\ 17'\ 00".8$	2.990910 (1)	11.67	7159	3.69	17, 18, 24
337094559	$22^h\ 22^m\ 32^s.6$	$+63^o\ 35'\ 10".6$	1.777515 (8)	9.98	7424	3.72	24
338159479[i]	$22^h\ 32^m\ 15^s.5$	$+64^o\ 58'\ 40".3$	1.414305 (1)	12.07	–	–	17, 18, 24
354926863	$02^h\ 37^m\ 46^s.2$	$+67^o\ 51'\ 19".9$	1.436540 (3)	10.98	7388	4.07	18, 19, 25
358613523[j]	$11^h\ 40^m\ 24^s.7$	$+80^o\ 14'\ 09".5$	1.327830 (5)	10.31	7271	4.28	14, 20, 21[n]
393894013[k]	$13^h\ 13^m\ 33^s.4$	$+47^o\ 47'\ 51".9$	0.816127 (4)	9.34	7866	4.19	22
396134795	$23^h\ 48^m\ 23^s.6$	$+36^o\ 18'\ 40".3$	2.586765 (4)	10.11	6946	3.80	17
396201681	$23^h\ 58^m\ 06^s.1$	$+67^o\ 36'\ 11".4$	7.039790 (1)	10.16	7767	–	17, 18, 24, 25
420114772	$19^h\ 21^m\ 43^s.2$	$+74^o\ 45'\ 45".5$	6.470060 (5)	10.47	7015	–	14–26, 41, 47
421714420	$21^h\ 38^m\ 45^s.8$	$+55^o\ 47'\ 29".9$	–	7.90	8820	3.81	16,17
428003183	$23^h\ 16^m\ 53^s.1$	$+44^o\ 29'\ 18".4$	0.742981 (7)	11.11	7345	4.05	16, 17
430808126	$22^h\ 15^m\ 58^s.4$	$+53^o\ 18'\ 43".1$	6.481440 (7)	11.56	8460	–	16, 17
440003271[l]	$00^h\ 10^m\ 03^s.2$	$+46^o\ 23'\ 25".1$	2.639210 (1)	7.51	8334	4.16	17
456905229[m]	$01^h\ 44^m\ 53^s.5$	$+19^o\ 51'\ 24".5$	1.692620 (8)	8.44	7041	–	17, 42, 43
467354611	$21^h\ 46^m\ 23^s.5$	$+77^o\ 22'\ 19".7$	–	9.76	6235	3.35	17, 19, 25, 26

[a]F1V (Avvakumova et al., 2013), [b]F0 + G9 IV (Svechnikov & Kuznetsova, 2004), [c]B9 (Avvakumova et al., 2013), [d]F1V + K6 (Avvakumova et al., 2013), [e]A9.5V + F3.5V (Avvakumova et al., 2013), [f]A5 (Avvakumova et al., 2013), [g]A2 + G6IV (Budding et al., 2004), [h]A0(Avvakumova et al., 2013), [i]A8 + G8IV (Budding et al., 2004), [j]A5 + G6IV (Budding et al., 2004), [k]A3 (Avvakumova et al., 2013), [l]A3 (Avvakumova et al., 2013), [m]F0 (Avvakumova et al., 2013), [n]14, 20, 21, 26, 40, 41

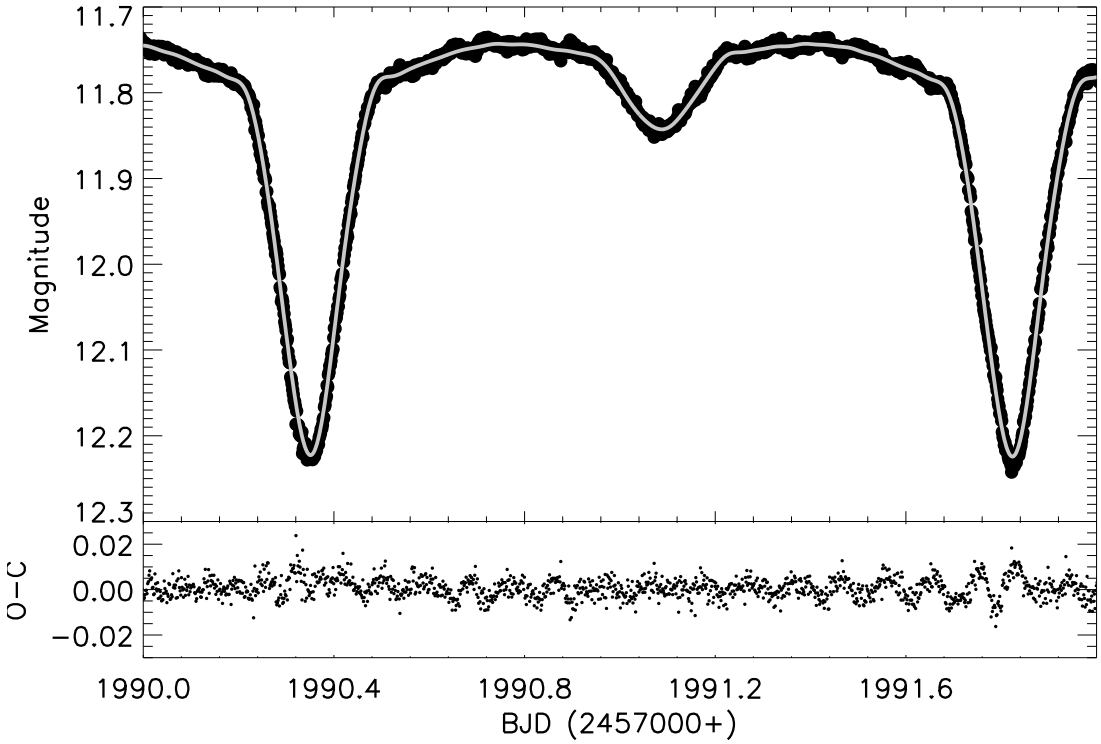

Fig. 1: Upper panel: the fit (grey line) of the orbital frequency and its harmonics to the TESS data of TIC 85600400. Lower panel: residuals.

no orbital frequency fit was applied, only the eclipse(s) was removed from the light curves and the rest was analysed.

After the binary variations were removed from the TESS data of all targets, we carried out a frequency analysis of the residuals in the second step of the analysis. The independent, harmonic and combination frequencies were searched for. During the analysis, the frequencies having a signal-to-noise (S/N) ratio over 4.5 were expected as significant. A typical significance limit for the detected frequencies is given as 4.0 by Breger et al. (1993). However, Baran & Koen (2021) showed that this limit should be higher for TESS data and by taking into account the results obtained in their study, we took the significance limit as 4.5. The analysis was carried out for a range of $\sim 4-80\,d^{-1}$ considering the typical pulsation period of δ Scuti stars (see, Sect. **??**). One object in our targets (TIC 396201681) clearly show long-term γ Doradus-type variation in its light curve. Therefore for this system the frequency analysis was performed for $\sim 0-80\,d^{-1}$ range of frequency, as γ Doradus stars typically exhibit pulsations with a frequency changing from $\sim$0.3 to 3 d^{-1} (Aerts et al., 2010). Consequently, the range and the number of the detected frequencies are listed in Table 2. The first five highest amplitude frequencies are also given in Table .4 for each target. The full table is given in electronic form. The frequency spectrum and the fits of the calculated frequencies to the observations are shown in Fig. 2 for one sample and in Fig. .5 for the others.

4 CALCULATING PHYSICAL PARAMETERS

For all systems, we calculated some physical parameters such as luminosity (L), absolute (M_V) and bolometric (M_{bol}) magnitudes. However, one should keep in mind that these parameters represent the binary

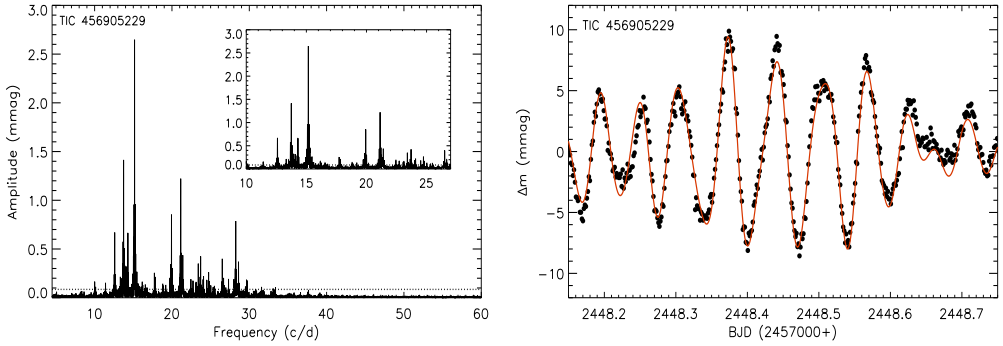

Fig. 2: Left panel: the frequency spectrum of TIC 456905229. The dashed line represents the 4.5-σ level. Right panel: theoretical fit (red solid line) to observed data (dots) for TIC 456905229.

system and do not belong to only one binary component. Before starting to calculate these parameters, we estimated flux densities of binary components to estimate the flux contributions of each component to the total. It is known that the area ratio of eclipses approximately gives the flux density ratio of the binary components (Binnendijk, 1960). In the primary eclipse (deeper one) the loss of light is more than the secondary eclipse, so in the primary eclipse, the star with the higher surface luminosity hence hotter is obscured by other. We call this star as primary (p) and the other cool and less luminous one as secondary (s) component. The area of primary (A_p) and secondary (A_s) eclipses were measured by using IRAF[2](Tody, 1986) splot task. The ratio of these areas is equal to flux density (I) ratio as shown in the following equation (Binnendijk, 1960):

$$\frac{A_p}{A_s} = \frac{I_p}{I_s} \tag{1}$$

The calculated I ratios are listed in Table 2. For some systems, there is only one eclipse available in the light curves, therefore flux ratio value could not be determined for these systems. As can be seen from the I ratios, in most systems I of the primary and secondary components close each other. We assumed that if the I ratio is over $\sim$4 the calculated physical parameters mostly belong to the primary component.

The physical parameters of all systems were calculated using the distance module and the Pogson equation. To compute these parameters, the distances of the systems were taken from the Gaia EDR3 (Gaia Collaboration et al., 2021) and also extinction coefficient (A_υ) was calculated utilizing the interstellar extinction maps of Amôres & Lépine (2005). First the M_V parameters were calculated by using the following equation:

$$V - M_V = 5logd - 5 + A_\upsilon \tag{2}$$

where V is the visual magnitude, d is the distance of the systems. After the M_V values were derived the M_{bol} parameters were computed taking into account the TIC $T_{\rm eff}$ values and bolometric corrections from Eker et al. (2020). If there is no $T_{\rm eff}$ value for a system we estimated this value from the target's spectral type by using the calibration between the spectral type and $T_{\rm eff}$ given by Gray (1992). Additionally, for TIC 13037534, $T_{\rm eff}$ determined from the spectral type-$T_{\rm eff}$ calibration was used. Then, the L parameters

[2] http://iraf.noao.edu/

were computed with the below equation:

$$\frac{L}{L_{\odot}} = 10^{(M_{bol\odot} - M_{bol})/2.5} \quad (3)$$

$M_{bol\odot}$ value is taken as $4^m.74$ according to IAU 2015 General Assembly resolution B2[3]. The calculated parameters are given in Table 2. Uncertainties of the computed parameters were estimated considering the errors in the input parameters. According to the I ratio of the primary and secondary components, these calculated parameters mostly represents the binary systems. However, there are some systems in which the given I ratio is over $\sim$4. In these systems the flux coming from the primary is significantly higher than the secondary and we assumed the calculated physical parameters mostly represents the hotter primary components and probably the pulsating one.

5 DISCUSSION

In this section, we examined some properties of our candidate DSEB.

5.1 Pulsation type

In this study, we present the analysis of some targets showing δ Scuti like variations. While determining the candidate DSEB, one of the important criteria was the $T_{\rm eff}$ of the eclipsing binary systems. However, we know that these $T_{\rm eff}$ values are an average of both binary components. So real $T_{\rm eff}$ of pulsating components, could be higher or cooler than the TIC $T_{\rm eff}$. In some systems, we found that the primary components have significantly more flux density compared to secondary (see, Table 2). In these systems[4], the $T_{\rm eff}$ mostly represents the hotter primary and probably the pulsating components. When we examined the $T_{\rm eff}$ values [5] of these systems, we found that their $T_{\rm eff}$ are in the range of the $T_{\rm eff}$ given for δ Scuti stars. Their pulsation amplitudes and frequencies are also consistent with the values given for δ Scuti stars (Aerts et al., 2010).

For the other systems which have the I ratio lover than 4, probably the TIC $T_{\rm eff}$ values are substantially different than the real $T_{\rm eff}$ values of the pulsating components. Inside the pulsating stars, there are two different types that exhibit frequencies like δ Scuti variables. One of them is β Cephei stars. The β Cephei stars mostly show frequencies between 3 and 12 d^{-1} and these pulsators have $B0-B3$ spectral type (Aerts et al., 2010). Although these pulsators are quite hotter than the δ Scuti variables, if a β Cephei star have a very cool binary component, the total $T_{\rm eff}$ of the system will be cooler than the value expected for the β Cephei stars. However, our targets have a $T_{\rm eff}$ value in a range of $\sim 6300-9100$ K and even if a β Cephei star has a cool binary component, the average $T_{\rm eff}$ of the binary system could not as low as our targets' $T_{\rm eff}$ range.

Another pulsating star group is Maia variables. The existence of Maia variables has not been exactly confirmed, however, for decades Maia variables are considered as a new group of pulsating stars (Aerts & Kolenberg, 2005; Balona et al., 2016; Balona & Ozuyar, 2020). The Maia variables are located between the β Cephei and δ Scuti stars, so they are cooler than β Cephei variables and hotter than the δ Scuti stars.

[3] https://www.iau.org/static/resolutions/IAU2015_English.pdf

[4] TIC 13037534, TIC 75593781, TIC 85600400, TIC 193774939, TIC 197757000, TIC 240962482, TIC 241013310, TIC 358613523, TIC 421714420

[5] for TIC 13037534, the spectral type was taken into account

Table 2: Calculated Physical Parameters, I Ratios of the Binary Components and the Range and the Number of the Detected Frequency. For TIC 430808126 Parameters could not be Calculated as It has no Parallax.

TIC number	A_v (mag) $\pm$ 0.002	M_V (mag)	M_{bol} (mag)	log (L/L$_\odot$)	I_p/I_s	Frequency range (d^{-1})	Number of frequency
8669966	0.031	0.716 ± 0.025	0.767 ± 0.025	1.610 ± 0.045	1.23	13.103 – 14.21	6
10057647	0.192	2.164 ± 0.032	2.237 ± 0.032	1.030 ± 0.052	1.40	13.77 – 51.41	23
13037534	0.720	0.571 ± 0.025	0.588 ± 0.024	1.668 ± 0.045	6.64	8.84 – 12.11	8
14948284	0.069	1.807 ± 0.024	1.883 ± 0.029	1.173 ± 0.044	1.20	8.09 – 24.92	21
48084398	0.048	0.555 ± 0.029	0.635 ± 0.032	1.674 ± 0.049	1.04	8.98 – 13.22	21
71613490	0.029	1.395 ± 0.032	1.441 ± 0.007	1.338 ± 0.052	1.04	24.47 – 32.34	19
72839144	0.077	1.416 ± 0.007	1.492 ± 0.028	1.329 ± 0.027	3.55	4.11	1
75593781	0.708	1.364 ± 0.029	1.355 ± 0.016	1.350 ± 0.049	4.47	46.11 – 57.94	15
78148497	0.663	1.324 ± 0.016	1.395 ± 0.032	1.367 ± 0.036	2.80	9.77 – 32.97	22
85600400	0.087	1.651 ± 0.032	1.724 ± 0.027	1.236 ± 0.052	3.85	9.70 – 19.97	17
116334565	0.809	0.849 ± 0.027	0.908 ± 0.031	1.557 ± 0.047	1.27	6.55 – 22.85	12
165618747	0.298	2.107 ± 0.031	2.162 ± 0.011	1.053 ± 0.051	1.97	15.13 – 40.18	28
172431974	0.047	1.557 ± 0.011	1.631 ± 0.032	1.273 ± 0.031	1.01	4.24 – 6.40	10
193774939	0.080	2.220 ± 0.033	4.974 ± 0.019	1.008 ± 0.053	5.16	16.59 – 31.21	21
197755658	0.029	2.074 ± 0.019	2.126 ± 0.013	1.066 ± 0.039	1.94	46.63 – 51.26	3
197757000	0.123	2.576 ± 0.013	2.657 ± 0.009	0.865 ± 0.033	4.46	21.17 – 41.98	21
240962482	0.190	1.689 ± 0.010	1.733 ± 0.007	1.221 ± 0.030	11.84	24.96 – 29.43	5
241013310	0.110	2.335 ± 0.007	2.414 ± 0.033	0.962 ± 0.027	4.02	4.82 – 14.77	4
256640561	0.079	0.823 ± 0.033	0.855 ± 0.007	1.567 ± 0.053	1.86	10.12 – 24.42	12
272822330	0.165	0.997 ± 0.007	1.066 ± 0.030	1.497 ± 0.027	1.91	14.03 – 20.34	11
289947843	0.083	0.912 ± 0.030	0.791 ± 0.012	1.531 ± 0.050	–	5.97 – 14.44	11
301909087	0.624	1.137 ± 0.012	1.218 ± 0.026	1.441 ± 0.032	1.04	5.58 – 17.44	10
305633328	0.245	1.680 ± 0.026	1.760 ± 0.014	1.224 ± 0.046	1.08	9.38 – 15.37	8
322428763	0.174	1.441 ± 0.014	1.517 ± 0.022	1.483 ± 0.014	1.53	11.99 – 49.78	11
327121759	0.726	1.374 ± 0.022	1.451 ± 0.011	1.346 ± 0.042	3.43	22.90 – 30.97	6
337094559	0.097	2.049 ± 0.011	2.114 ± 0.061	1.077 ± 0.031	1.78	7.86 – 19.47	8
338159479	0.292	2.332 ± 0.062	2.383 ± 0.011	0.963 ± 0.081	2.01	21.75 – 28.51	17
354926863	0.298	2.755 ± 0.011	2.822 ± 0.007	0.794 ± 0.031	1.06	4.66 – 39.11	18
358613523	0.097	2.813 ± 0.007	2.885 ± 0.034	0.771 ± 0.027	5.16	24.59 – 46.44	15
393894013	0.044	2.216 ± 0.035	2.250 ± 0.023	1.010 ± 0.055	1.49	8.55 – 69.65	19
396134795	0.628	1.290 ± 0.023	1.371 ± 0.038	1.380 ± 0.043	1.63	14.20 – 28.47	7
396201681	0.184	1.595 ± 0.038	1.638 ± 0.071	1.258 ± 0.058	1.14	1.21 – 23.52	11
420114772	0.127	0.656 ± 0.071	0.736 ± 0.016	1.634 ± 0.091	1.05	5.02 – 41.95	30
421714420	0.097	-0.083 ± 0.016	-0.154 ± 0.014	1.929 ± 0.036	10.00	4.01 – 53.19	11
428003183	0.106	2.438 ± 0.014	2.506 ± 0.015	0.921 ± 0.034	2.56	12.93 – 32.77	22
430808126	–	–	–	–	1.07	5.26 – 27.63	22
440003271	0.030	1.524 ± 0.026	1.510 ± 0.026	1.287 ± 0.046	1.10	12.19 – 37.33	19
456905229	0.048	2.060 ± 0.074	2.139 ± 0.074	1.072 ± 0.094	1.12	10.13 – 33.39	44
467354611	0.094	1.825 ± 0.023	1.166 ± 0.043	1.876 ± 0.027	–	11.58 – 31.04	41

Additionally, Maia variables demonstrate oscillations approximately in a similar frequency range with the δ Scuti stars (Balona et al., 2016; Balona & Ozuyar, 2020). Even the existence of Maia variables has not been approved, if they are a new type of variables, they could be a member of binary systems and seen cooler

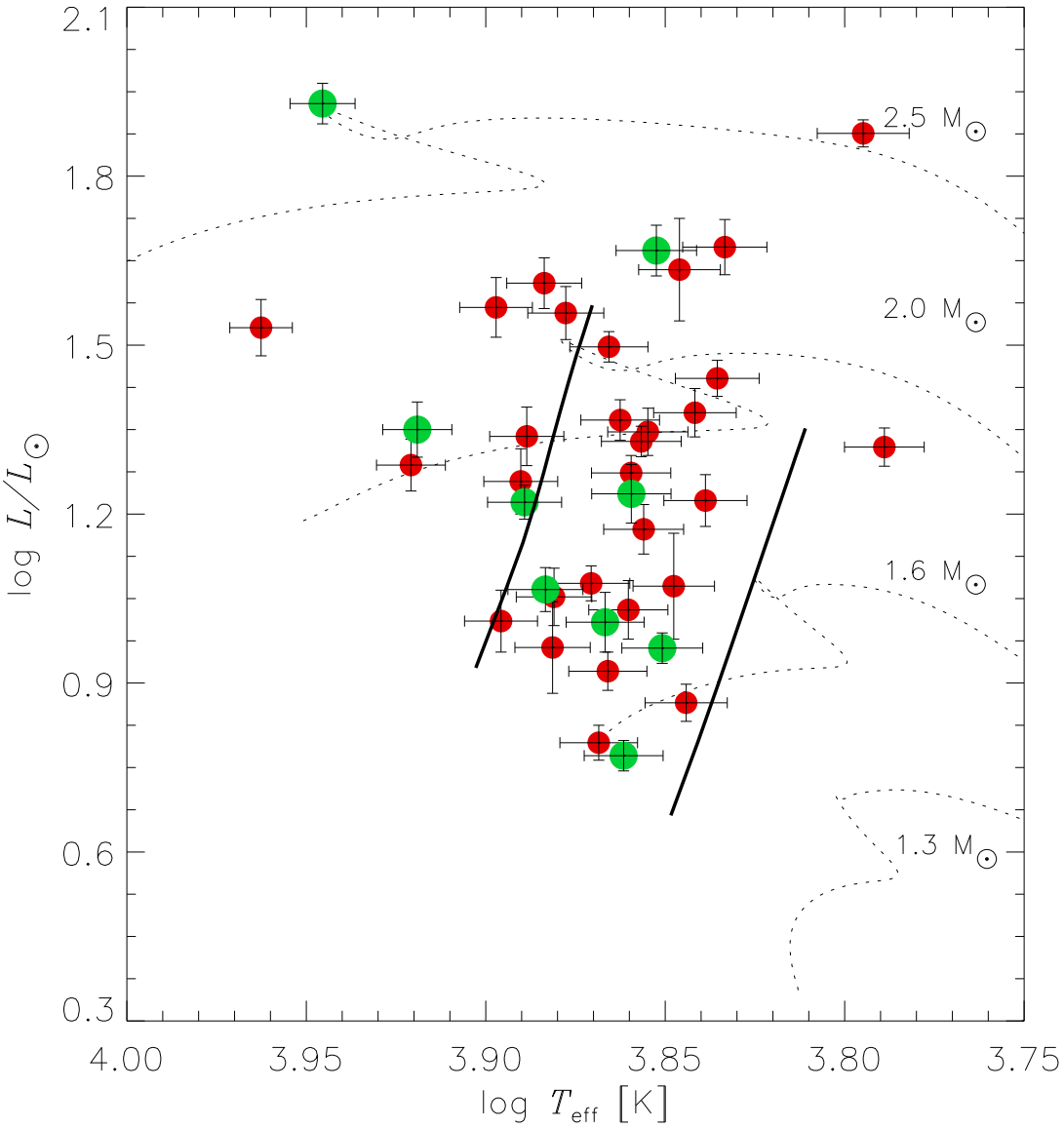

Fig. 3: Positions of the targets in the H-R diagram. Green dots represent the systems having I ratio higher than $\sim$4, while red smaller dots shows the other systems. The solid and dashed lines are the borders of the δ Scuti instability strip (Dupret et al., 2005) and the evolutionary tracks taken from the MESA Isochrones and Stellar Tracks (MIST) (Paxton et al., 2011; Dotter, 2016; Choi et al., 2016), respectively.

than expected if a Maia variable has a cooler binary component. In this case, they could be considered as a δ Scuti variable. To have an idea about the variability type of our targets, their positions in the Hertzsprung-Russell (H-R) diagram should be examined by considering the I ratios. Therefore, we showed the positions of our systems in the H-R diagram by using the parameters given in Table 1 and Table 2.

As can be seen from Fig. 3, most of the systems, which have an I ratio over around 4, are located in the δ Scuti instability strip and for these systems, we assumed the L and $T_{\rm eff}$ mostly represent the primary, probably the pulsating, binary component. Inside these systems, there is one object (TIC 421714420) that is placed beyond the hot border of δ Scuti instability strip. In a detailed study of *Kepler* field δ Scuti and related stars, Uytterhoeven et al. (2011) showed that there are some real δ Scuti variables located beyond

the borders of the δ Scuti instability strip. However, this system is noticeable far from the δ Scuti instability strip, and very close to the place where Maia variables are located (Balona & Ozuyar, 2020). Therefore we classified this system as a candidate of Maia variable in an eclipsing binary. There is another system located beyond the hotter border of δ Scuti stars, TIC 289947843, unfortunately, we could not measure the I ratio for this system because there is not enough data. For the other systems having I ratio <4 the L value of the pulsating component should be lower than the calculated one and depending on $T_{\rm eff}$ of the other binary component the $T_{\rm eff}$ of the pulsating star could be lower or higher than the used in the H-R diagram. Taking into account these conditions, we could say that most pulsating components could be located inside the δ Scuti instability strip however it is difficult to have an idea about the variability of the systems considering this. Therefore, as a result of this examination, we classified 38 systems as candidate DSEB and one of them, TIC 421714420, as a Maia candidate in an eclipsing binary system.

5.2 Consistency with the known relationship for DSEBs

DSEB have been investigated for a long time and it was shown that there are some relationships between the pulsation period, amplitude and the other parameters such as P_{orb}, R and $\log g$ (Kahraman Aliçavuş et al., 2017; Liakos & Niarchos, 2017). For DSEB, the well-known relationship is between the $\rm P_{orb}$ and $\rm P_{puls}$. In the latest study of Kahraman Aliçavuş et al. (2017), it was shown that known DSEB obey this relationship within error bars. We examined whether our candidate systems suit this relationship. In this section, we only investigate the candidate DSEB. As can be seen from Fig.4, most of our candidates are consistent with the relationship within errors. There are a few objects placed outside of the 1-σ level, TIC 72839144, TIC 172431974, TIC 197755658 and TIC 241013310. The reason for these could be the additional effect in the binary system such as mass transfer between binary components if these systems are DSEB.

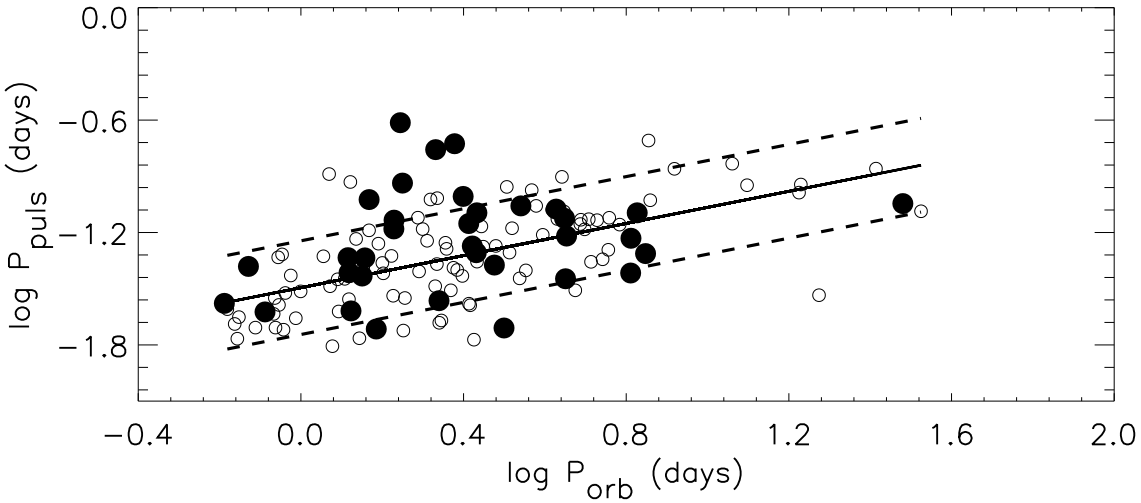

Fig. 4: Consistency of the candidate DSEB with $\rm P_{orb} - P_{puls}$ relationship. The filled and empty circles represent our candidate and the known DSEB (Kahraman Aliçavuş et al., 2017), respectively. The solid and dashed lines show the correlation and 1-σ level, respectively.

More relationships between the $\rm P_{puls}$ and other parameters are given by Kahraman Aliçavuş et al. (2017) for detached and semi-detached systems. These parameters help us approximately estimate some physical

Table 3: Calculated Parameters from the Given Relationships by Kahraman Aliçavuş et al. (2017).

TIC number	$\log g$ (cgs)	R ($R_\odot$)	M ($M_\odot$)
8669966	3.65 ± 0.20	3.53 ± 0.39	2.07 ± 0.30
10057647	4.41 ± 0.24	1.39 ± 0.24	1.85 ± 0.38
13037534	3.51 ± 0.28	3.93 ± 0.51	1.85 ± 0.40
14948284	3.93 ± 0.10	2.74 ± 0.32	2.38 ± 0.10
48084398	3.56 ± 0.26	3.80 ± 0.47	1.93 ± 0.36
71613490	4.10 ± 0.11	2.25 ± 0.05	2.39 ± 0.06
75593781	4.59 ± 0.34	0.88 ± 0.39	1.13 ± 0.36
78148497	3.59 ± 0.24	3.70 ± 0.44	1.98 ± 0.34
116334565	3.53 ± 0.28	3.87 ± 0.49	1.88 ± 0.38
165618747	4.37 ± 0.22	1.52 ± 0.20	1.97 ± 0.34
193774939	3.97 ± 0.12	2.62 ± 0.12	2.40 ± 0.19
197757000	4.35 ± 0.20	1.57 ± 0.18	2.03 ± 0.30
240962482	4.16 ± 0.14	2.10 ± 0.03	2.36 ± 0.09
256640561	3.44 ± 0.32	4.11 ± 0.56	1.75 ± 0.44
272822330	3.79 ± 0.12	3.14 ± 0.28	2.25 ± 0.20
289947843	3.69 ± 0.18	3.41 ± 0.36	2.13 ± 0.28
301909087	3.64 ± 0.22	3.57 ± 0.40	2.05 ± 0.32
305633328	3.45 ± 0.32	4.10 ± 0.56	1.75 ± 0.44
322428763	3.59 ± 0.24	3.70 ± 0.44	1.98 ± 0.34
327121759	4.04 ± 0.10	2.44 ± 0.17	2.41 ± 0.22
338159479	4.13 ± 0.10	2.17 ± 0.01	2.38 ± 0.09
354926863	3.98 ± 0.10	2.61 ± 0.12	2.40 ± 0.17
358613523	4.43 ± 0.26	1.32 ± 0.26	1.77 ± 0.42
393894013	4.44 ± 0.26	1.30 ± 0.26	1.74 ± 0.44
396134795	3.68 ± 0.10	3.44 ± 0.37	2.11 ± 0.28
396201681	3.94 ± 0.10	2.72 ± 0.15	2.38 ± 0.17
420114772	4.11 ± 0.10	2.24 ± 0.05	2.39 ± 0.07
421714420	4.27 ± 0.16	1.78 ± 0.24	2.20 ± 0.22
428003183	4.05 ± 0.10	2.40 ± 0.06	2.41 ± 0.11
430808126	3.81 ± 0.06	3.09 ± 0.26	2.27 ± 0.18
440003271	3.87 ± 0.14	2.90 ± 0.21	2.34 ± 0.14
456905229	3.73 ± 0.16	3.31 ± 0.33	2.18 ± 0.24
467354611	3.71 ± 0.16	3.35 ± 0.34	2.16 ± 0.26

parameters of the δ Scuti pulsating components in eclipsing binary systems. As we do not know the Roche geometry of our systems we could not classify the binary configurations of our targets. However, for both detached and semi-detached binary configurations, some relationships give a good correlation between the P_{puls} such as $\log g$ and radius (R) of the pulsating component. Therefore, we calculated $\log g$ and R parameters of our systems using the equations given in the study of Kahraman Aliçavuş et al. (2017). In this calculation, we excluded the systems found outside of the $P_{orb} - P_{puls}$ relationship. The computed $\log g$ and R parameters are listed in Table 3. By utilizing the calculated $\log g$ and R, we also estimated the mass (M) values of the pulsating component. These values are also given in Table 3. It should keep in mind that these parameters are just an estimation and do not give exact values and the real errors should be higher.

6 CONCLUSIONS

In this study, we present the results of our northern TESS field search to discover new eclipsing binaries with δ Scuti components. We first determined 39 targets and examined the pulsational properties (pulsation amplitude and frequencies) of these systems after removing the eclipsing variations. In addition to determining pulsation amplitude and frequencies, we also estimated the I ratios of binary components to find how much binary components contribute to total flux relative to each other. To estimate whether our systems could be DSEB or not, we also controlled the positions of the targets in the H-R diagram. For this, we calculated L parameters of the systems. By considering the positions of the systems in the H-R diagram and the I ratios, we showed that one of our targets (TIC 421714420) could be a candidate of Maia variable in an eclipsing binary system. The other targets in the study are classified as candidate DSEB. However, to be sure about the positions of the systems in the H-R diagram and the real $T_{\rm eff}$ values of them, detailed spectroscopic analysis and binary modelling are necessary. With the spectroscopy the $T_{\rm eff}$ value of each binary component can be derived and with the binary modelling, the real L parameters could be reached.

We know that the pulsating eclipsing binary systems are quite important to deeply understand stellar systems. An increasing number of these kinds of systems would contribute to improving our knowledge about the stellar evolution and structure. Therefore, this study would be useful for both probing stellar structure, evolution and understanding the pulsation behaviour of oscillating stars in eclipsing binary systems.

Acknowledgements This work has been supported in part by the Scientific and Technological Research Council (TUBITAK) under the grant number 120F330. The TESS data presented in this paper were obtained from the Mikulski Archive for Space Telescopes (MAST). FKA thanks Prof. Gerald HANDLER for showing how to clean binarity with a phenomenological fit. Funding for the TESS mission is provided by the NASA Explorer Program. This work has made use of data from the European Space Agency (ESA) mission Gaia (http://www.cosmos.esa.int/gaia), processed by the Gaia Data Processing and Analysis Consortium (DPAC, http://www.cosmos.esa.int/web/gaia/dpac/consortium). Funding for the DPAC has been provided by national institutions, in particular the institutions participating in the Gaia Multilateral Agreement. This research has made use of the SIMBAD data base, operated at CDS, Strasbourq, France.

References

Aerts, C. & Kolenberg, K. 2005, A&A, 431, 615. doi:10.1051/0004-6361:20041325

Aerts, C., Christensen-Dalsgaard, J., & Kurtz, D. W. 2010, Asteroseismology, Astronomy and Astrophysics Library. ISBN 978-1-4020-5178-4. Springer Science+Business Media B.V., 2010, p.

Amôres, E. B. & Lépine, J. R. D. 2005, AJ, 130, 659. doi:10.1086/430957

Avvakumova, E. A., Malkov, O. Y., & Kniazev, A. Y. 2013, Astronomische Nachrichten, 334, 860. doi:10.1002/asna.201311942

Balona, L. A., Engelbrecht, C. A., Joshi, Y. C., et al. 2016, MNRAS, 460, 1318. doi:10.1093/mnras/stw1038

Balona, L. A. & Ozuyar, D. 2020, MNRAS, 493, 5871. doi:10.1093/mnras/staa670

Baran, A. S. & Koen, C. 2021, Acta Astronomica, 71, 113. doi:10.32023/0001-5237/71.2.3

Binnendijk, L. 1960, Philadelphia, University of Pennsylvania Press [1960]

Borucki, W. J., Koch, D., Basri, G., et al. 2010, Science, 327, 977. doi:10.1126/science.1185402

Breger, M., Stich, J., Garrido, R., et al. 1993, A&A, 271, 482

Budding, E., Erdem, A., Çiçek, C., et al. 2004, A&A, 417, 263. doi:10.1051/0004-6361:20034135

Dupret, M.-A., Grigahcène, A., Garrido, R., et al. 2005, A&A, 435, 927. doi:10.1051/0004-6361:20041817

Eker, Z., Soydugan, F., Bilir, S., et al. 2020, MNRAS, 496, 3887. doi:10.1093/mnras/staa1659

Fuller, J., Kurtz, D. W., Handler, G., et al. 2020, MNRAS, 498, 5730. doi:10.1093/mnras/staa2376

Gaia Collaboration, Brown, A. G. A., Vallenari, A., et al. 2021, A&A, 649, A1. doi:10.1051/0004-6361/202039657

Gray, D. F. 1992, Camb. Astrophys. Ser., Vol. 20,

Handler, G., Kurtz, D. W., Rappaport, S. A., et al. 2020, Nature Astronomy, 4, 684. doi:10.1038/s41550-020-1035-1

Kahraman Aliçavuş, F., Soydugan, E., Smalley, B., et al. 2017, MNRAS, 470, 915. doi:10.1093/mnras/stx1241

Kahraman Aliçavuş, F., Handler, G., Aliçavuş, F., et al. 2022, MNRAS, 510, 1413. doi:10.1093/mnras/stab3515

Kurtz, D. W., Handler, G., Rappaport, S. A., et al. 2020, MNRAS, 494, 5118. doi:10.1093/mnras/staa989

Lacy, M., Ridgway, S. E., Sajina, A., et al. 2015, ApJ, 802, 102. doi:10.1088/0004-637X/802/2/102

Lampens, P. 2021, Galaxies, 9, 28. doi:10.3390/galaxies9020028

Lenz, P. & Breger, M. 2005, Communications in Asteroseismology, 146, 53. doi:10.1553/cia146s53

Liakos, A. & Niarchos, P. 2017, MNRAS, 465, 1181. doi:10.1093/mnras/stw2756

Lovekin, C. C. & Guzik, J. A. 2017, ApJ, 849, 38. doi:10.3847/1538-4357/aa8e01

Mkrtichian, D. E., Kusakin, A. V., Rodriguez, E., et al. 2004, A&A, 419, 1015. doi:10.1051/0004-6361:20040095

Paxton, B., Bildsten, L., Dotter, A., et al. 2011, ApJS, 192, 3. doi:10.1088/0067-0049/192/1/3

Choi, J., Dotter, A., Conroy, C., et al. 2016, ApJ, 823, 102. doi:10.3847/0004-637X/823/2/102

Dotter, A. 2016, ApJS, 222, 8. doi:10.3847/0067-0049/222/1/8

Ricker, G. R., Winn, J. N., Vanderspek, R., et al. 2014, Proc. SPIE, 9143, 914320. doi:10.1117/12.2063489

Rodríguez, E. & Breger, M. 2001, A&A, 366, 178. doi:10.1051/0004-6361:20000205

Saio, H., Kurtz, D. W., Takata, M., et al. 2015, MNRAS, 447, 3264. doi:10.1093/mnras/stu2696

Soydugan, E., İbanoğlu, C., Soydugan, F., et al. 2006, MNRAS, 366, 1289. doi:10.1111/j.1365-2966.2005.09889.x

Southworth, J. 2013, A&A, 557, A119. doi:10.1051/0004-6361/201322195

Southworth, J. 2021, The Observatory, 141, 282

Stassun, K. G., Oelkers, R. J., Paegert, M., et al. 2019, AJ, 158, 138. doi:10.3847/1538-3881/ab3467

Svechnikov, M. A. & Kuznetsova, E. F. 2004, VizieR Online Data Catalog, V/124

Tempesti, P. 1971, Information Bulletin on Variable Stars, 596, 1

Tody, D. 1986, Proc. SPIE, 627, 733. doi:10.1117/12.968154

Uytterhoeven, K., Moya, A., Grigahcène, A., et al. 2011, A&A, 534, A125. doi:10.1051/0004-6361/201117368

Table .4: The List of the First Five Highest Amplitude Frequency Detected in This Study. The Full List of the Frequencies is Given in Electronic Form.

	Frequency (d^{-1})	Amplitude (mmag)	Phase (rad)	S/N		Frequency (d^{-1})	Amplitude (mmag)	Phase (rad)	S/N		Frequency (d^{-1})	Amplitude (mmag)	Phase (rad)	S/N
	TIC 8669966					TIC 10057647					TIC 13037534			
ν_1	13.62189 ± 0.00015	0.717 ± 0.005	0.5562 ± 0.0011	62	ν_1	40.11281 ± 0.00019	0.727 ± 0.007	0.2288 ± 0.0015	54	ν_1	11.10889 ± 0.00004	0.526 ± 0.012	0.8332 ± 0.0036	20
ν_2	13.14363 ± 0.00017	0.618 ± 0.005	0.0358 ± 0.0013	61	ν_2	30.95924 ± 0.00020	0.686 ± 0.007	0.1324 ± 0.0015	69	ν_2	8.84272 ± 0.00006	0.459 ± 0.012	0.3634 ± 0.0048	24
ν_3	13.32788 ± 0.00038	0.278 ± 0.005	0.0784 ± 0.0028	26	ν_3	38.78309 ± 0.00028	0.481 ± 0.007	0.8545 ± 0.0022	31	ν_3	9.74327 ± 0.00006	0.323 ± 0.012	0.4381 ± 0.0055	13
ν_4	13.03191 ± 0.00042	0.251 ± 0.005	0.0809 ± 0.0031	25	ν_4	43.60348 ± 0.00034	0.399 ± 0.007	0.4591 ± 0.0027	28	ν_4	10.63240 ± 0.00015	0.210 ± 0.012	0.2293 ± 0.0045	8
ν_5	13.73165 ± 0.00049	0.217 ± 0.005	0.5787 ± 0.0036	19	ν_5	36.01630 ± 0.00048	0.283 ± 0.007	0.6612 ± 0.0037	24	ν_5	10.41897 ± 0.00026	0.207 ± 0.019	0.8755 ± 0.0495	8
	TIC 14948284					TIC 48084398					TIC 71613490			
ν_1	20.31697 ± 0.00019	3.130 ± 0.028	0.7751 ± 0.0014	22	ν_1	11.88739 ± 0.00006	1.099 ± 0.006	0.5054 ± 0.0008	30	ν_1	25.98838 ± 0.00049	0.323 ± 0.007	0.9887 ± 0.0035	24
ν_2	11.20278 ± 0.00021	2.776 ± 0.028	0.1298 ± 0.0016	20	ν_2	9.49467 ± 0.00006	1.009 ± 0.006	0.9585 ± 0.0009	24	ν_2	31.57531 ± 0.00054	0.289 ± 0.007	0.8029 ± 0.0039	26
ν_3	20.11472 ± 0.00038	1.567 ± 0.028	0.5509 ± 0.0029	11	ν_3	11.41491 ± 0.00007	0.861 ± 0.006	0.9264 ± 0.0010	25	ν_3	30.81604 ± 0.00057	0.274 ± 0.007	0.2540 ± 0.0041	23
ν_4	18.05449 ± 0.00038	1.541 ± 0.028	0.0802 ± 0.0029	16	ν_2+ν_3-ν_1	9.02219 ± 0.00008	0.784 ± 0.006	0.3972 ± 0.0011	19	ν_4	31.33778 ± 0.00061	0.257 ± 0.007	0.7478 ± 0.0043	22
ν_5	17.67646 ± 0.00048	1.247 ± 0.028	0.1414 ± 0.0036	14	ν_5	11.02949 ± 0.00010	0.632 ± 0.006	0.1951 ± 0.0014	18	ν_5	26.25839 ± 0.00065	0.242 ± 0.007	0.9569 ± 0.0046	15
	TIC 72839144					TIC 75593781					TIC 78148497			
ν_1	4.11102 ± 0.00133	0.328 ± 0.020	0.8042 ± 0.0098	6.0	ν_1	51.91704 ± 0.00011	1.544 ± 0.023	0.1718 ± 0.0024	46	ν_1	12.44590 ± 0.00009	1.383 ± 0.017	0.3311 ± 0.0020	39
					ν_2	48.85966 ± 0.00018	0.914 ± 0.023	0.8996 ± 0.0040	30	ν_2	16.39778 ± 0.00014	0.900 ± 0.017	0.5090 ± 0.0031	19
					ν_3	52.40034 ± 0.00022	0.754 ± 0.023	0.5367 ± 0.0048	22	ν_3	24.48400 ± 0.00019	0.662 ± 0.017	0.2477 ± 0.0042	16
					ν_4	47.75704 ± 0.00028	0.588 ± 0.023	0.1146 ± 0.0062	20	ν_4	23.67636 ± 0.00018	0.677 ± 0.017	0.9442 ± 0.0041	16
					ν_5	50.61103 ± 0.00026	0.622 ± 0.023	0.7971 ± 0.0058	19	ν_5	26.07247 ± 0.00020	0.616 ± 0.017	0.5684 ± 0.0045	17
	TIC 85600400					TIC 116334565					TIC 165618747			
ν_1	10.57549 ± 0.00018	1.666 ± 0.027	0.6049 ± 0.0026	29	ν_1	11.42838 ± 0.00007	2.212 ± 0.117	0.4961 ± 0.0005	36	ν_1	37.87282 ± 0.00039	0.765 ± 0.025	0.5868 ± 0.0060	23
ν_2	11.01141 ± 0.00021	1.386 ± 0.027	0.2475 ± 0.0031	24	ν_2	14.76193 ± 0.00007	1.360 ± 0.117	0.8032 ± 0.0005	20	ν_2	37.54370 ± 0.00039	0.675 ± 0.025	0.4108 ± 0.0059	20
ν_3	16.63944 ± 0.00025	1.171 ± 0.027	0.3368 ± 0.0037	22	ν_3	15.15892 ± 0.00008	0.1207 ± 0.117	0.7195 ± 0.0006	17	ν_3	35.11748 ± 0.00060	0.474 ± 0.025	0.1010 ± 0.0090	14
ν_4	11.39975 ± 0.00025	1.183 ± 0.027	0.8613 ± 0.0037	20	ν_4	7.97122 ± 0.00010	1.212 ± 0.117	0.7470 ± 0.0007	17	ν_4	23.54175 ± 0.00056	0.430 ± 0.025	0.9865 ± 0.0084	14
ν_5	17.99572 ± 0.00030	0.971 ± 0.027	0.3860 ± 0.0045	22	ν_5	6.54611 ± 0.00012	1.073 ± 0.117	0.7175 ± 0.0008	13	ν_5	30.49806 ± 0.00069	0.414 ± 0.025	0.6068 ± 0.0103	12

Table .4: Continuation.

	Frequency (d^{-1})	Amplitude (mmag)	Phase (rad)	S/N		Frequency (d^{-1})	Amplitude (mmag)	Phase (rad)	S/N		Frequency (d^{-1})	Amplitude (mmag)	Phase (rad)	S/N
	TIC 172431974					TIC 193774939					TIC 197755658			
ν_1	5.32323 ± 0.00015	1.854 ± 0.026	0.3324 ± 0.0022	42	ν_1	21.59652 ± 0.00014	0.825 ± 0.010	0.6836 ± 0.0020	38	ν_1	51.25620 ± 0.00044	0.562 ± 0.024	0.9177 ± 0.0067	22
ν_2	4.27899 ± 0.00053	0.528 ± 0.026	0.5921 ± 0.0078	7	ν_2	26.67014 ± 0.00014	0.783 ± 0.010	0.7211 ± 0.0021	45	ν_2	46.63643 ± 0.00080	0.310 ± 0.024	0.7649 ± 0.0121	11
ν_3	5.12970 ± 0.00054	0.443 ± 0.026	0.6626 ± 0.0093	10	ν_3	16.69181 ± 0.00017	0.642 ± 0.010	0.9187 ± 0.0026	42	ν_3	49.19415 ± 0.00097	0.256 ± 0.024	0.7373 ± 0.0147	8
ν_4	4.24755 ± 0.00058	0.489 ± 0.026	0.7757 ± 0.0085	7	ν_4	23.58869 ± 0.00039	0.290 ± 0.010	0.2894 ± 0.0058	17					
ν_5	4.69256 ± 0.00079	0.356 ± 0.026	0.4970 ± 0.0116	7	ν_5	18.01112 ± 0.00049	0.228 ± 0.010	0.4957 ± 0.0073	14					
	TIC 197757000					TIC 240962482					TIC 241013310			
ν_1	36.65383 ± 0.00021	0.859 ± 0.016	0.3463 ± 0.0030	35	ν_1	27.98413 ± 0.00035	1.147 ± 0.016	0.2308 ± 0.0022	23	ν_1	5.72370 ± 0.00025	0.615 ± 0.014	0.9089 ± 0.0035	13
ν_2	29.57429 ± 0.00029	0.606 ± 0.016	0.9506 ± 0.0023	23	ν_2	27.65528 ± 0.00064	0.633 ± 0.016	0.5763 ± 0.0040	12	ν_2	6.25826 ± 0.00041	0.370 ± 0.014	0.3633 ± 0.0058	8
ν_3	26.64726 ± 0.00033	0.541 ± 0.016	0.4796 ± 0.0048	19	ν_3	27.29194 ± 0.00071	0.567 ± 0.016	0.0469 ± 0.0045	10	ν_3	14.76784 ± 0.00042	0.361 ± 0.014	0.4021 ± 0.0060	17
ν_4	21.64643 ± 0.00038	0.466 ± 0.016	0.2506 ± 0.0056	18	ν_4	29.43289 ± 0.00082	0.490 ± 0.016	0.9475 ± 0.0052	11	ν_4	4.81999 ± 0.00057	0.264 ± 0.014	0.4349 ± 0.0082	5
ν_5	38.32894 ± 0.00043	0.411 ± 0.016	0.3283 ± 0.0063	17	ν_5	24.96472 ± 0.00078	0.517 ± 0.016	0.7146 ± 0.0049	17					
	TIC 256640561					TIC 272822330					TIC 289947843			
ν_1	10.11866 ± 0.00018	0.217 ± 0.004	0.8695 ± 0.0028	36	ν_1	16.55851 ± 0.00001	0.506 ± 0.013	0.7901 ± 0.0042	11	ν_1	14.42398 ± 0.00003	0.357 ± 0.003	0.1029 ± 0.0015	41
ν_2	16.27639 ± 0.00037	0.105 ± 0.004	0.2941 ± 0.0057	19	ν_2	17.89061 ± 0.00001	0.471 ± 0.013	0.7731 ± 0.0045	10	ν_2	11.61625 ± 0.00005	0.224 ± 0.003	0.9873 ± 0.0023	22
ν_3	15.11399 ± 0.00039	0.100 ± 0.004	0.6635 ± 0.0060	19	ν_3	15.37946 ± 0.00001	0.332 ± 0.013	0.9197 ± 0.0064	8	ν_3	11.62266 ± 0.00005	0.217 ± 0.003	0.1661 ± 0.0024	21
ν_4	17.43972 ± 0.00043	0.090 ± 0.004	0.0847 ± 0.0067	16	ν_4	20.33903 ± 0.00001	0.326 ± 0.013	0.7286 ± 0.0065	7	ν_4	14.42912 ± 0.00008	0.150 ± 0.003	0.5904 ± 0.0035	17
ν_5	11.00822 ± 0.00063	0.062 ± 0.004	0.8177 ± 0.0097	10	ν_5	17.61348 ± 0.00001	0.306 ± 0.013	0.7254 ± 0.0070	6	ν_5	12.40031 ± 0.00008	0.146 ± 0.003	0.1397 ± 0.0035	15
	TIC 301909087					TIC 305633328					TIC 322428763			
ν_1	13.31209 ± 0.00019	2.861 ± 0.023	0.1732 ± 0.0013	39	ν_1	10.17360 ± 0.00037	0.806 ± 0.026	0.2727 ± 0.0052	19	ν_1	12.44685 ± 0.00002	27.487 ± 0.024	0.2984 ± 0.0001	380
ν_2	11.41486 ± 0.00041	1.341 ± 0.023	0.0983 ± 0.0028	25	ν_2	14.84142 ± 0.00043	0.699 ± 0.026	0.2635 ± 0.0060	18	$2\nu_1$	24.89370 ± 0.00013	3.479 ± 0.024	0.0780 ± 0.0011	81
ν_3	10.42865 ± 0.00057	0.964 ± 0.023	0.9806 ± 0.0038	20	ν_3	15.31862 ± 0.00055	0.541 ± 0.026	0.1905 ± 0.0078	15	ν_3	15.92382 ± 0.00037	1.259 ± 0.024	0.9422 ± 0.0030	26
ν_4	13.09508 ± 0.00061	0.896 ± 0.023	0.5211 ± 0.0041	13	ν_4	15.36912 ± 0.00094	0.320 ± 0.026	0.2315 ± 0.0132	9	$3\nu_1$	37.34056 ± 0.00038	1.223 ± 0.024	0.4383 ± 0.0031	54
ν_5	11.63832 ± 0.00068	0.803 ± 0.023	0.9980 ± 0.0046	14	ν_5	11.05172 ± 0.00119	0.253 ± 0.026	0.1454 ± 0.0166	5	ν_5	12.14271 ± 0.00062	0.749 ± 0.024	0.9277 ± 0.0050	11

Table .4: Continuation.

	Frequency (d^{-1})	Amplitude (mmag)	Phase (rad)	S/N		Frequency (d^{-1})	Amplitude (mmag)	Phase (rad)	S/N		Frequency (d^{-1})	Amplitude (mmag)	Phase (rad)	S/N
	TIC 327121759					TIC 337094559					TIC 338159479			
ν_1	23.65750 ± 0.00008	1.016 ± 0.030	0.3121 ± 0.0048	18	ν_1	8.63508 ± 0.00035	1.561 ± 0.026	0.6307 ± 0.0027	16	ν_1	27.06439 ± 0.00006	1.347 ± 0.024	0.0505 ± 0.0029	54
ν_2	24.50198 ± 0.00009	0.872 ± 0.030	0.7576 ± 0.0056	17	ν_2	8.26695 ± 0.00054	1.020 ± 0.026	0.2042 ± 0.0041	11	ν_2	23.55252 ± 0.00004	0.642 ± 0.015	0.5789 ± 0.0038	23
ν_3	22.90103 ± 0.00011	0.690 ± 0.030	0.4459 ± 0.0070	13	ν_3	7.86106 ± 0.00056	0.990 ± 0.026	0.8082 ± 0.0043	12	ν_3	24.96688 ± 0.00004	0.461 ± 0.014	0.8664 ± 0.0049	18
ν_4	23.56995 ± 0.00013	0.573 ± 0.030	0.6620 ± 0.0085	10	$16\nu_o rb{+}2\nu_1\text{-}\nu_3$	18.46141 ± 0.00069	0.923 ± 0.026	0.3725 ± 0.0053	8	ν_4	28.51068 ± 0.00005	0.390 ± 0.014	0.3448 ± 0.0058	15
ν_5	30.96969 ± 0.00016	0.482 ± 0.030	0.2912 ± 0.0101	10	ν_5	10.20012 ± 0.00069	0.802 ± 0.026	0.5700 ± 0.0062	6	ν_5	23.06376 ± 0.00008	0.280 ± 0.014	0.7468 ± 0.0084	10
	TIC 354926863					TIC 358613523					TIC 393894013			
ν_1	21.66089 ± 0.00002	1.813 ± 0.013	0.3126 ± 0.0011	89	ν_1	41.55243 ± 0.00024	0.465 ± 0.011	0.0551 ± 0.0039	24	ν_1	42.07023 ± 0.00056	0.468 ± 0.013	0.6493 ± 0.0043	14
ν_2	23.97610 ± 0.00010	0.311 ± 0.013	0.8778 ± 0.0064	15	ν_2	32.82261 ± 0.00036	0.309 ± 0.011	0.7414 ± 0.0058	17	ν_2	50.86278 ± 0.00060	0.444 ± 0.013	0.3516 ± 0.0045	15
ν_3	29.74307 ± 0.00011	0.291 ± 0.013	0.2144 ± 0.0068	20	ν_3	30.25640 ± 0.00038	0.298 ± 0.011	0.6099 ± 0.0060	16	ν_3	52.98499 ± 0.00074	0.359 ± 0.013	0.3011 ± 0.0056	13
ν_4	7.55377 ± 0.00011	0.278 ± 0.013	0.2867 ± 0.0071	15	ν_4	36.31599 ± 0.00047	0.240 ± 0.011	0.3481 ± 0.0075	13	ν_4	45.70912 ± 0.00077	0.345 ± 0.013	0.3654 ± 0.0058	12
ν_5	17.71561 ± 0.00013	0.238 ± 0.013	0.5979 ± 0.0084	14	ν_5	45.76655 ± 0.00050	0.224 ± 0.011	0.7536 ± 0.0080	14	ν_5	40.74380 ± 0.00087	0.305 ± 0.013	0.7169 ± 0.0066	10
	TIC 396134795					TIC 396201681					TIC 420114772			
ν_1	14.19761 ± 0.00025	2.507 ± 0.026	0.6492 ± 0.0016	31	ν_1	2.09187 ± 0.00003	3.890 ± 0.011	0.7970 ± 0.0004	90	ν_1	26.07772 ± 0.00012	0.402 ± 0.009	0.9829 ± 0.0035	35
ν_2	23.06211 ± 0.00052	1.190 ± 0.026	0.1993 ± 0.0035	20	ν_2	1.96327 ± 0.00004	3.284 ± 0.011	0.4973 ± 0.0005	72	ν_2	19.65159 ± 0.00012	0.400 ± 0.009	0.4690 ± 0.0035	34
ν_3	27.50727 ± 0.00087	0.711 ± 0.026	0.3443 ± 0.0058	9	ν_3	20.53793 ± 0.00006	1.973 ± 0.011	0.3971 ± 0.0009	93	ν_3	21.29354 ± 0.00012	0.390 ± 0.009	0.8579 ± 0.0036	36
ν_4	28.46996 ± 0.00097	0.637 ± 0.026	0.1605 ± 0.0065	8	ν_4	25.52245 ± 0.00008	1.433 ± 0.011	0.0180 ± 0.0012	68	ν_4	22.36688 ± 0.00014	0.338 ± 0.009	0.0937 ± 0.0041	32
ν_5	25.46129 ± 0.00162	0.380 ± 0.026	0.8832 ± 0.0109	8	ν_5	20.07776 ± 0.00014	0.873 ± 0.011	0.8036 ± 0.0020	48	ν_5	22.30157 ± 0.00015	0.300 ± 0.009	0.8503 ± 0.0047	28
	TIC 421714420					TIC 428003183					TIC 430808126			
ν_1	33.00852 ± 0.00001	0.566 ± 0.005	0.8806 ± 0.0013	94	ν_1	24.04691 ± 0.00025	0.921 ± 0.021	0.4706 ± 0.0037	21	ν_1	17.01396 ± 0.00030	0.780 ± 0.022	0.9924 ± 0.0045	21
ν_2	16.63040 ± 0.00001	0.223 ± 0.005	0.2679 ± 0.0033	38	ν_2	22.69924 ± 0.00051	0.592 ± 0.021	0.2310 ± 0.0074	15	ν_2	21.80517 ± 0.00044	0.540 ± 0.022	0.1305 ± 0.0064	12
ν_3	53.15438 ± 0.00001	0.172 ± 0.005	0.0092 ± 0.0043	33	ν_3	14.00456 ± 0.00040	0.590 ± 0.021	0.4984 ± 0.0058	14	ν_3	17.04825 ± 0.00047	0.501 ± 0.022	0.8969 ± 0.0069	13
ν_4	20.91822 ± 0.00001	0.100 ± 0.005	0.9778 ± 0.0073	17	ν_4	30.70567 ± 0.00044	0.532 ± 0.021	0.7363 ± 0.0064	11	ν_4	5.25878 ± 0.00058	0.405 ± 0.022	0.8720 ± 0.0086	10
ν_5	24.82455 ± 0.00001	0.101 ± 0.005	0.5483 ± 0.0073	14	ν_5	14.04931 ± 0.00066	0.458 ± 0.021	0.5547 ± 0.0096	11	ν_5	15.14783 ± 0.00067	0.351 ± 0.022	0.7665 ± 0.0099	10

Table .4: Continuation.

	Frequency (d^{-1})	Amplitude (mmag)	Phase (rad)	S/N		Frequency (d^{-1})	Amplitude (mmag)	Phase (rad)	S/N		Frequency (d^{-1})	Amplitude (mmag)	Phase (rad)	S/N
	TIC 440003271					TIC 456905229					TIC 467354611			
ν_1	18.71653 ± 0.00031	1.204 ± 0.016	0.1117 ± 0.0021	36	ν_1	15.16456 ± 0.00003	2.646 ± 0.007	0.7014 ± 0.0004	167	ν_1	14.90235 ± 0.00001	3.905 ± 0.008	0.5206 ± 0.0004	166
ν_2	15.61934 ± 0.00032	1.192 ± 0.016	0.8186 ± 0.0021	36	ν_2	13.64681 ± 0.00005	1.468 ± 0.007	0.1107 ± 0.0008	82	ν_2	13.61211 ± 0.00001	3.039 ± 0.007	0.9023 ± 0.0005	152
ν_3	14.94367 ± 0.00040	0.940 ± 0.016	0.4500 ± 0.0027	29	ν_3	21.13332 ± 0.00006	1.226 ± 0.007	0.7881 ± 0.0009	58	ν_3	14.13054 ± 0.00001	2.320 ± 0.009	0.5640 ± 0.0005	97
ν_4	16.02039 ± 0.00054	0.697 ± 0.016	0.9872 ± 0.0036	21	ν_4	19.93937 ± 0.00009	0.852 ± 0.007	0.5775 ± 0.0013	46	ν_4	14.09850 ± 0.00001	1.035 ± 0.007	0.4843 ± 0.0011	43
ν_5	20.54519 ± 0.00058	0.657 ± 0.016	0.0864 ± 0.0038	20	ν_5	28.24970 ± 0.00009	0.809 ± 0.007	0.4093 ± 0.0014	46	ν_5	12.21896 ± 0.00001	0.702 ± 0.011	0.5071 ± 0.0019	51

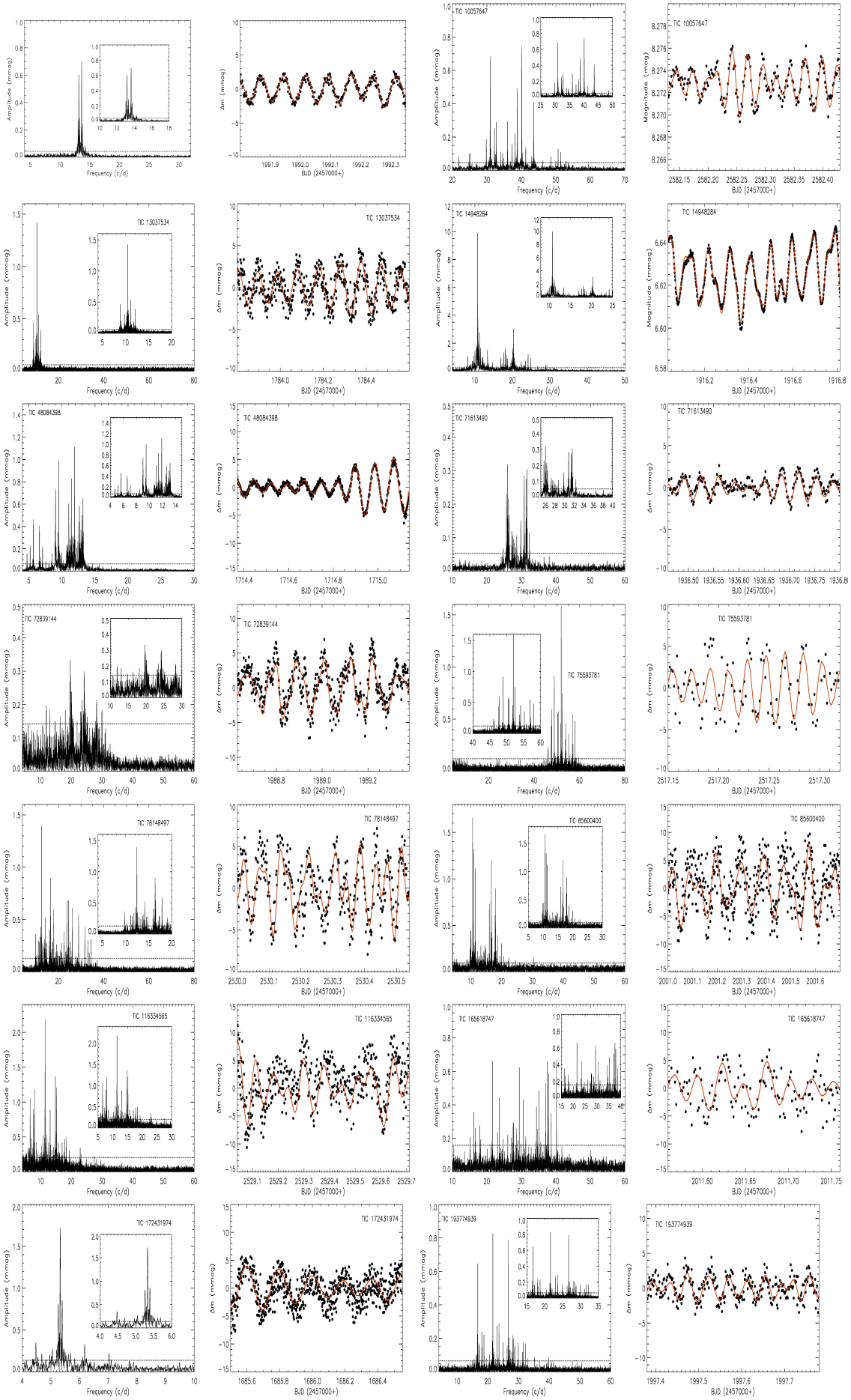

Fig. .5: Amplitude spectra of the targets and the theoretical frequency fit (red solid lines) to the observations. Dotted lines represent the 4.5-σ level.

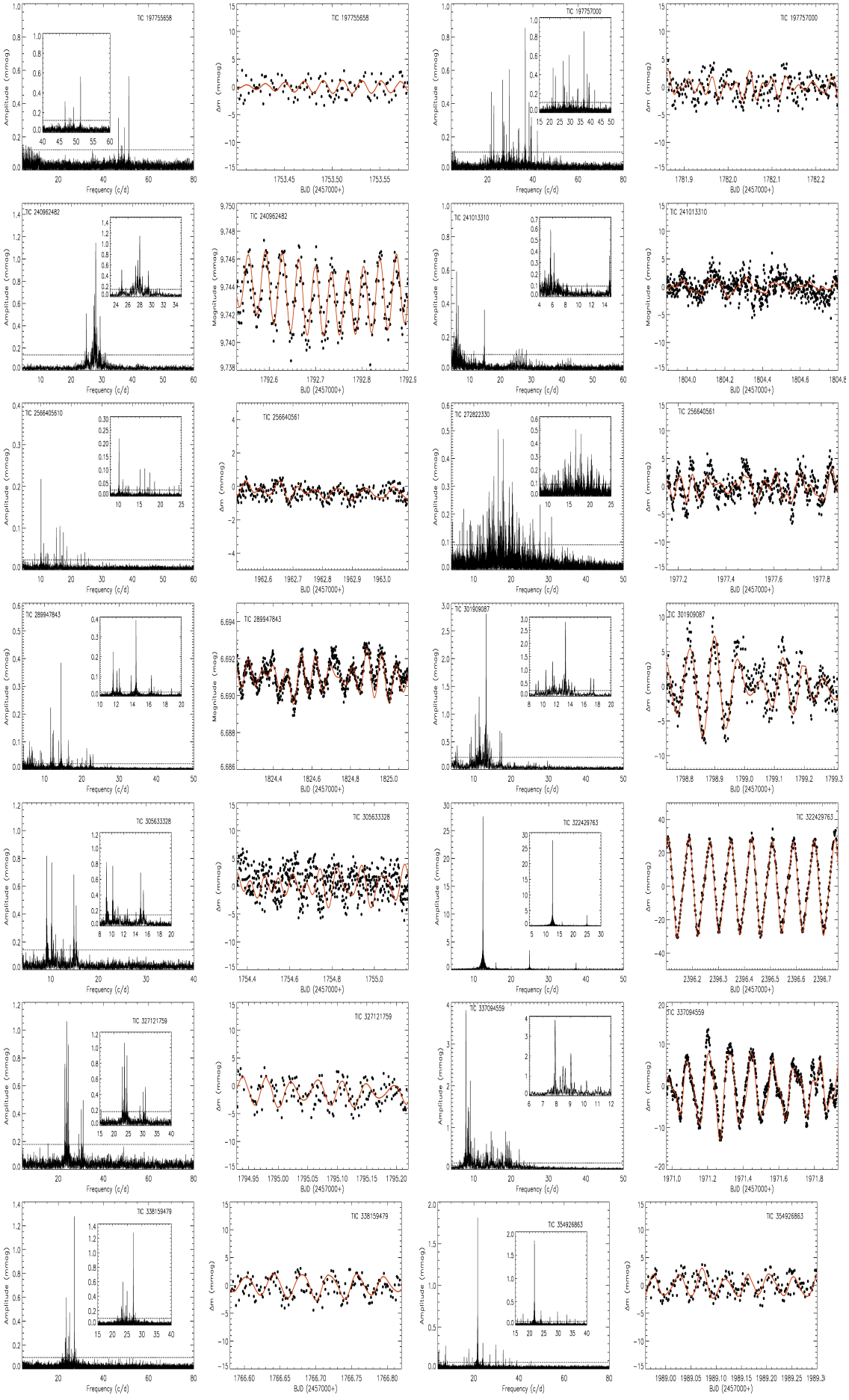

Fig. .5: Continuation.

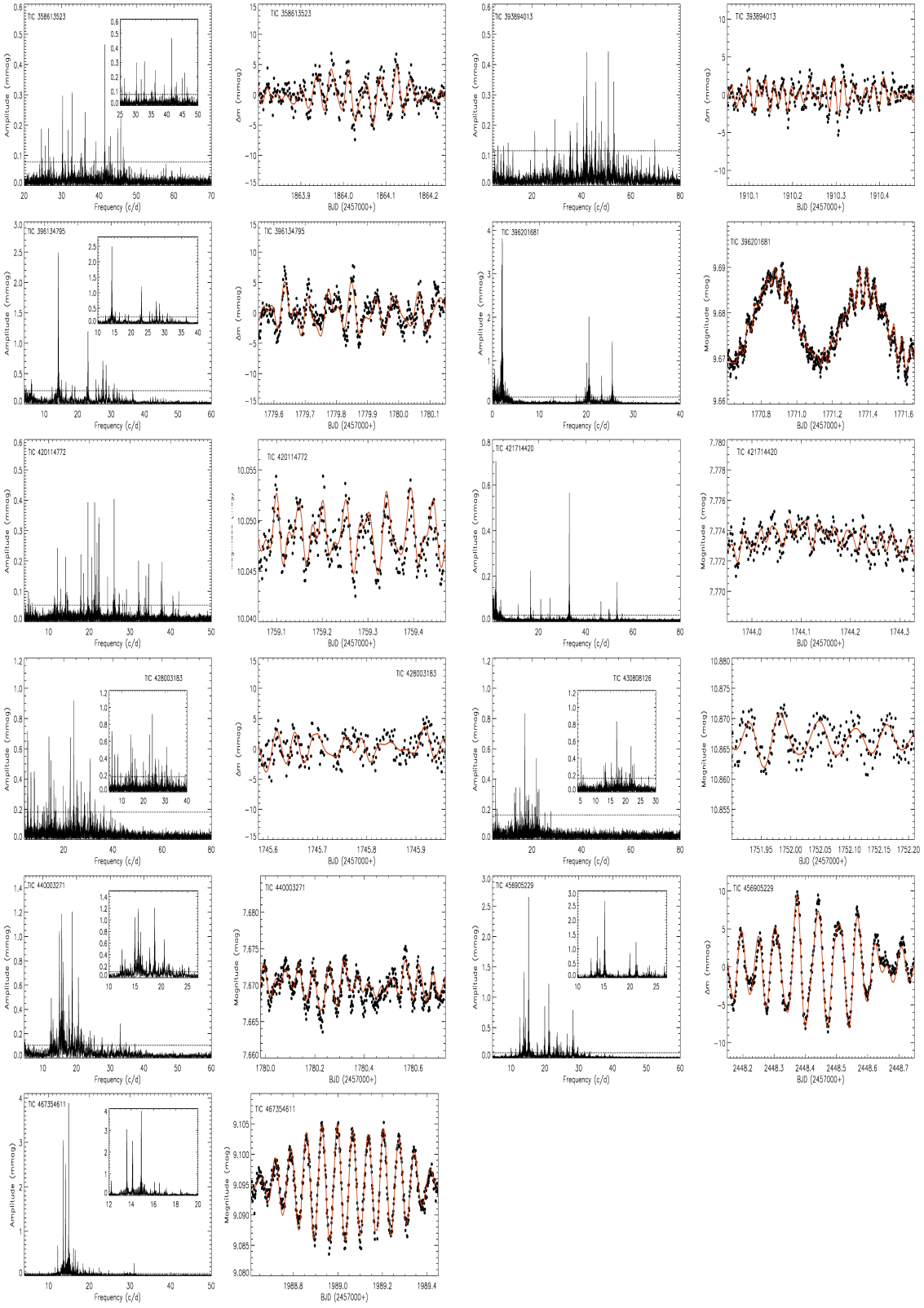

Fig. .5: Continuation.